Atlantic-Pacific seesaw and its role in outgassing CO 2 during Heinrich events

L. Menviel, M. England, K. Meissner, A. Mouchet, J. Yu

PALEOCEANOGRAPHY, VOL. 29, 58–70, doi:10.1002/2013PA002542, 2014

Atlantic-Pacific seesaw and its role in outgassing CO_2 during Heinrich events

L. Menviel,[1,2] M. H. England,[1,2] K. J. Meissner,[1,2] A. Mouchet,[3,4] and J. Yu[5]

Received 31 July 2013; revised 4 December 2013; accepted 5 December 2013; published 30 January 2014.

[1] Paleoproxy records indicate that a marked weakening of the Atlantic Meridional Overturning Circulation (AMOC) during Heinrich events was often accompanied by a notable atmospheric CO_2 increase. However, previous modeling studies display conflicting atmospheric CO_2 responses to an AMOC shutdown. Here we use model simulations combined with paleoproxy records to show that depending on the deep and bottom water transport in the Northern and Southern Pacific Ocean during an AMOC weakening, the ocean can act either as a sink or a source of carbon. Results from idealized meltwater experiments as well as from a transient experiment covering Heinrich stadial 4 suggest that a shutdown of the AMOC during Heinrich stadials 4 (HS4) and 1 (HS1) led to an enhancement of Antarctic Bottom Water (AABW) and North Pacific Deep Water (NPDW) transport. We show that enhanced deep and bottom water transport in the Pacific Ocean ventilates deep Pacific carbon through the Southern Ocean, thus contributing to a rise in atmospheric CO_2. This mechanism yields a good agreement between paleoproxy records and modeling results, thus highlighting the possible establishment of an Atlantic-Pacific seesaw during Heinrich stadials. Enhanced AABW and NPDW transport could account for most of the observed atmospheric CO_2 increase during HS4 and for about 30% of the atmospheric CO_2 increase during HS1.

Citation: Menviel, L., M. H. England, K. J. Meissner, A. Mouchet, and J. Yu (2014), Atlantic-Pacific seesaw and its role in outgassing CO_2 during Heinrich events, *Paleoceanography*, *29*, 58–70, doi:10.1002/2013PA002542.

1. Introduction

[2] The last glacial period and the last deglaciation were punctuated by millennial-scale events during which the Atlantic Meridional Overturning Circulation (AMOC) weakened substantially [*McManus et al.*, 2004]. These events, called Heinrich events [*Vidal et al.*, 1997], occurred most likely due to the addition of meltwater in the North Atlantic as a result of ice sheet instabilities [*Heinrich*, 1988]. A weakening of the AMOC during Heinrich events had a strong impact on the climate around the North Atlantic region [*Dansgaard et al.*, 1993; *Bond*, 1993] and, via oceanic and atmospheric teleconnections, it also led to significant climate change in the tropics [*Deplazes et al.*, 2013], across Asia [*Tada et al.*, 1999; *Wang et al.*, 2001], and through the bipolar seesaw effect, in Antarctica [*Blunier and Brook*, 2001]. However, not all Heinrich stadials display similar characteristics. Paleoproxy records suggest that Heinrich stadial 4 (HS4, 40–38 ka B.P.) [*Hemming*, 2004], was associated with a strong cooling over Greenland [*Huber et al.*, 2006] and the North Atlantic [*Bard*, 2002; *Martrat et al.*, 2007] as well as with a significant atmospheric CO_2 increase at the beginning of the cool phase [*Bereiter et al.*, 2012; *Ahn et al.*, 2012]. Paleorecords display little coherency regarding the amplitude and the timing of Heinrich stadial 3, maybe because in contrast to other Heinrich events, it originated from the Fennoscandian ice sheet [*Elliot et al.*, 1998; *Snoeckx et al.*, 1999; *Grousset et al.*, 2000] . Heinrich stadial 2 also displays a muted climatic response without any discernible change in atmospheric CO_2 [*Ahn and Brook*, 2008]. Finally Heinrich stadial 1 (HS1), which occurred right at the beginning of the last deglaciation, is associated with an atmospheric CO_2 increase, but it is still unclear how much of this increase is due to the abrupt circulation changes and how much is due to other processes linked to the deglaciation. Oceanic $\Delta^{14}C$ [*Skinner et al.*, 2010; *Burke and Robinson*, 2012] and atmospheric $\delta^{13}C$ records [*Schmitt et al.*, 2012] indicate that greater Southern Ocean ventilation during HS1 could have led to the observed atmospheric CO_2 rise.

[3] Previous studies examined either the terrestrial carbon response [*Scholze et al.*, 2003; *Köhler et al.*, 2005],

Additional supporting information may be found in the online version of this article.

[1]Climate Change Research Centre, University of New South Wales, Sydney, New South Wales, Australia.
[2]ARC Centre of Excellence for Climate System Science, Sydney, New South Wales, Australia.
[3]Laboratoire des Sciences du Climat et de l'Environnement (LSCE), IPSL-CEA-CNRS-UVSQ, Gif-sur-Yvette, France.
[4]Astrophysics, Geophysics and Oceanography Department, Université de Liège, Liège, Belgium.
[5]Research School of Earth Sciences, Australian National University, Canberra, ACT, Australia.

Corresponding author: L. Menviel, Climate Change Research Centre, University of New South Wales, Sydney, NSW 2052, Australia. (l.menviel@unsw.edu.au)

0883-8305/14/10.1002/2013PA002542

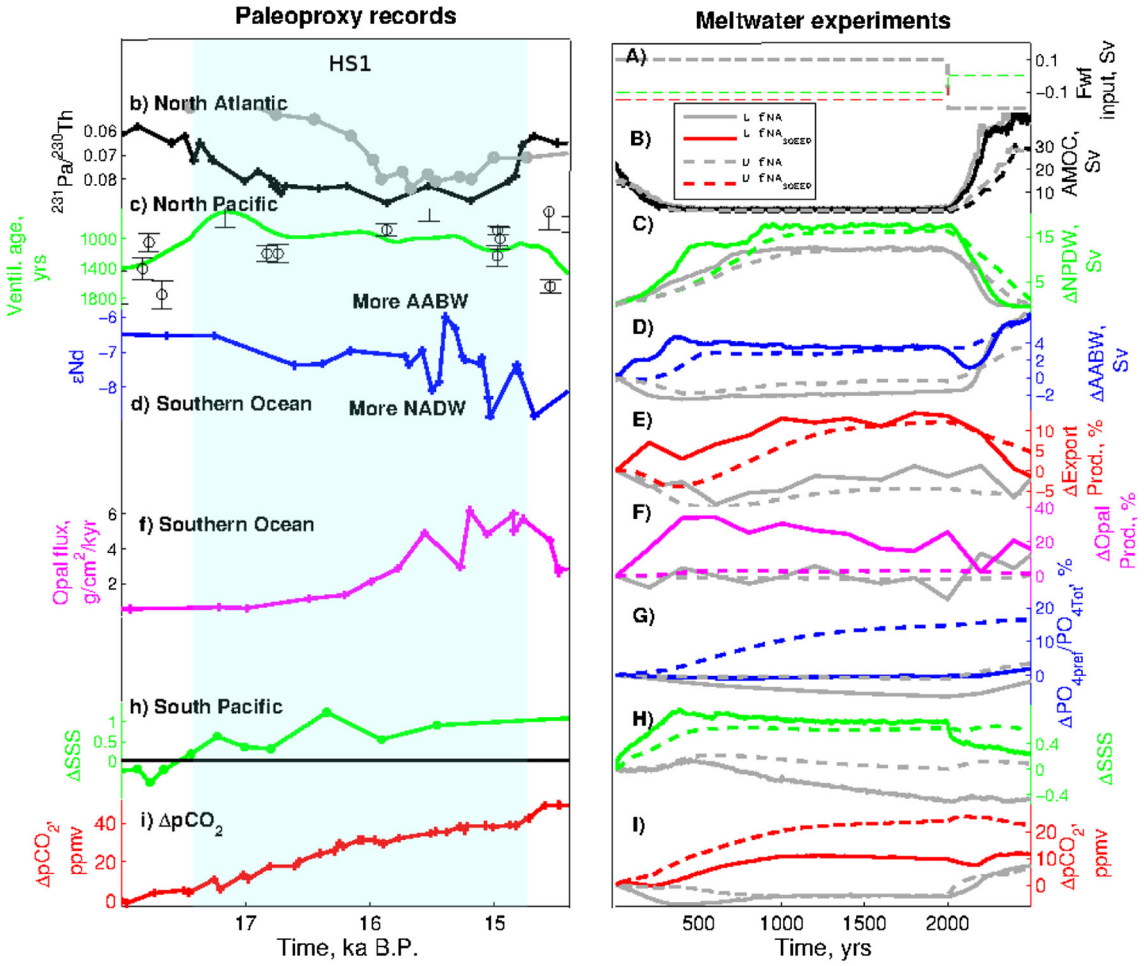

Figure 1. Paleoproxy records of Heinrich event 1 compared to idealized meltwater experiments: (left) Paleoproxy records (where available) and (right) modeling results for experiments L-fNA (solid grey), L-fNA$_{SOEEP}$ (solid red color), U-fNA (dashed grey), and U-fNA$_{SOEEP}$ (dashed red color). Time series of (A) Freshwater flux (Sv) in the North Atlantic (grey) for all experiments and over the Southern Ocean and the EEP for L-fNA$_{SOEEP}$ (red) and U-fNA$_{SOEEP}$ (green). (b) Maximum overturning circulation during the deglaciation as recorded in marine sediment cores from the North Atlantic by *McManus et al.* [2004] (black) and *Gherardi et al.* [2005] (grey); (B) Maximum overturning circulation in the North Atlantic (Sv); (c) Compilation of ventilation ages (years) from Northwestern Pacific sediment cores [*Okazaki et al.*, 2010], Benthic-Planktonic foraminifera ages (black circles) with 1σ error bar, and smoothed spline interpolation of averaged BF-PF and projection ages (green); (C) North Pacific Deep Water transport anomaly (Sv); (d) ϵNd from core RC11-83 in the South Atlantic [*Piotrowski et al.*, 2005]; Note that the 6 ka B.P. value is –9.3, thus indicating a greater proportion of AABW relative to NADW during HS1; (D) Antarctic Bottom Water transport anomaly in the Pacific Ocean (Sv). The AABW is calculated here as the maximum strength of the overturning in the abyssal cell at 35°S and positive ΔAABW indicates stronger AABW; (E) global export production anomalies (%) (f) opal flux (g/cm^2/kyr) in marine sediment core TNO57-13PC from the South Atlantic [*Anderson et al.*, 2009]; (F) opal production anomalies (%) for LOVECLIM and marine export production anomalies (%) for the UVic ESCM over the South Atlantic (50°W–20°E, 42°S–60°S); (G) Changes in PO_{4Pref}/PO_{4Tot} (%); (h) SSS anomalies in the South Pacific ocean as derived from planktic $\delta^{18}O$ for core MD03-2611 [*Calvo et al.*, 2007] (see section 2); (H) SSS anomaly averaged over the South Pacific Ocean (120°E–200°E, 35°S–50°S); (i) atmospheric CO_2 anomalies (ppmv) as recorded in the European Project for Ice Coring in Antarctica Dome C ice core, Antarctica [*Parrenin et al.*, 2013]; (I) simulated atmospheric CO_2 anomaly (ppmv). Please note that the ice core and simulated ΔpCO_2 are on different scales.

the marine carbon cycle response [*Marchal et al.*, 1999; *Chikamoto et al.*, 2012], or the combined marine and terrestrial carbon response [*Obata*, 2007; *Schmittner et al.*, 2007; *Menviel et al.*, 2008a; *Schmittner and Galbraith*, 2008; *Bozbiyik et al.*, 2011; *Bouttes et al.*, 2012; *Huiskamp and Meissner*, 2012; *Matsumoto and Yokoyama*, 2013] to an AMOC shutdown. While some modeling studies concluded that the oceanic carbon content increased as a result

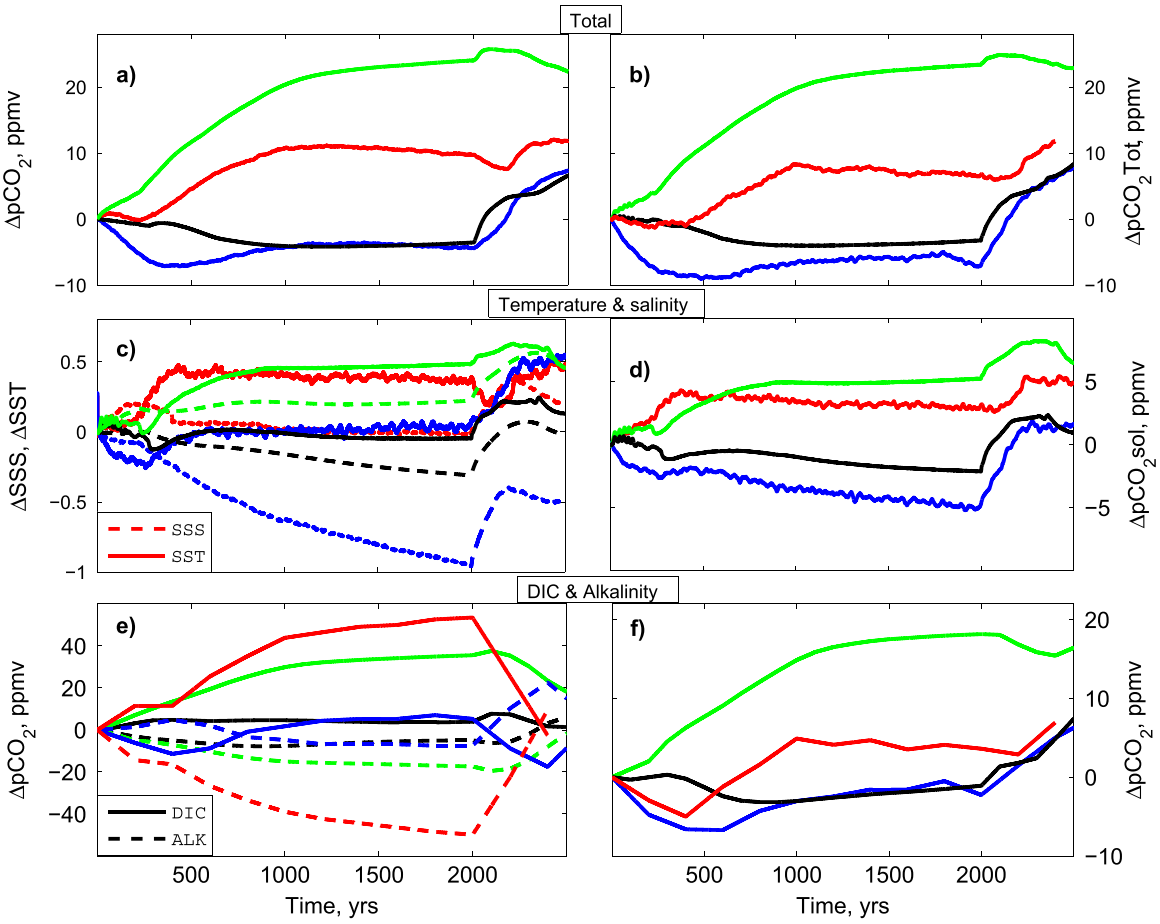

Figure 2. Decomposition of CO_2 changes for idealized meltwater experiments: Time series of (a) simulated atmospheric CO_2 anomaly (ppmv); (b) changes in atmospheric CO_2 (ppmv) as calculated from the different contributions of ΔSSS, ΔSST, ΔALK, and ΔDIC (see section 2); (c) global SSS (dashed, g/kg) and SST (solid, °C) anomalies; (d) changes in atmospheric CO_2 (ppmv) as calculated from ΔSSS and ΔSST; (e) changes in atmospheric CO_2 (ppmv) resulting from global surface ΔDIC (solid) and ΔALK (dashed); (f) changes in atmospheric CO_2 (ppmv) resulting from the combined contribution of ΔDIC and ΔALK for standard meltwater experiments performed with LOVECLIM (L-fNA, blue) and the UVic ESCM (U-fNA, black) as well as meltwater experiments with a negative freshwater flux in the Southern Ocean and EEP for LOVECLIM (L-fNA$_{SOEEP}$, red) and the UVic ESCM (U-fNA$_{SOEEP}$, green).

of an AMOC shutdown [*Obata*, 2007; *Menviel et al.*, 2008a; *Bozbiyik et al.*, 2011; *Chikamoto et al.*, 2012], others suggested the opposite [*Marchal et al.*, 1999; *Schmittner et al.*, 2007; *Schmittner and Galbraith*, 2008; *Bouttes et al.*, 2012; *Matsumoto and Yokoyama*, 2013]. Most of the studies [*Marchal et al.*, 1999; *Bouttes et al.*, 2012; *Matsumoto and Yokoyama*, 2013] which concluded that the oceanic carbon content decreased as a result of an AMOC shutdown, applied global salt compensation in their experimental design. Simulating a shutdown of the AMOC due to an ice sheet collapse presents some technical difficulties as the volume of the ocean remains constant in most climate models. In addition, freshwater pathways in the North Atlantic are affected by model resolution [*Condron and Winsor*, 2011; *Spence et al.*, 2013]. It is thus likely that due to a combination of experimental design, model resolution, and other model biases, standard meltwater experiments might not capture the past variability of Pacific deep and bottom water masses accurately.

[4] Here we show that knowledge of changes not only in North Atlantic Deep Water (NADW) but also in North Pacific Deep Water (NPDW) and Antarctic Bottom Water (AABW) transport is required to fully understand the responses of the global climate and oceanic carbon cycle during Heinrich events. We further suggest that a strengthening of AABW and NPDW formation during HS1 and HS4 caused a carbon release from the deep Pacific Ocean, thus leading to an atmospheric CO_2 increase.

2. Methods

2.1. Model and Experimental Design

[5] In this study we perform experiments with two Earth System Models of Intermediate Complexity: LOVECLIM 1.1 [*Goosse et al.*, 2010] and the University of Victoria Earth System Climate Model (UVic ESCM) v2.9 [*Weaver et al.*, 2001]. The ocean component of LOVECLIM (CLIO)

Table 1. Main Results of Idealized Experiments. Changes in Atmospheric CO_2 and Carbon Content (GtC) in the Atlantic, Pacific, Indian, and Arctic Basins as Well as in the Southern Ocean at Model Years 1990–2000 Compared to the LGM Control Run[a]

Exp.	ΔpCO_2 (ppmv)	ΔC Atl. (GtC)	ΔC Pac. (GtC)	ΔC Ind. (GtC)	ΔC SO (GtC)	ΔC Arctic (GtC)
LOVECLIM						
L-fNA	–4.4	366 (216)	–397 (–66)	–40	24	57
L-fNA$_{SOEEP}$	9.8	344 (172)	–430 (–218)	–29	31	50
UVic						
U-fNA	–3.5	280 (167)	–344 (–147)	–12	41	40
U-fNA$_{SOEEP}$	24	302 (124)	–408 (–314)	11	–7	48

[a]For the Atlantic and Pacific basins, the first number represents changes integrated over all depths and the number in brackets represents changes integrated over the deep ocean only (≥2000 m).

consists of a free-surface primitive equation model with a horizontal resolution of 3° longitude, 3° latitude, and 20 depth layers. The atmospheric component (ECBilt) is a spectral T21, three-level model based on quasi geostrophic equations of motion. LOVECLIM also includes a dynamic-thermodynamic sea ice model, a land surface scheme, a dynamic global vegetation model (VECODE), and a marine carbon cycle model (LOCH) [*Menviel*, 2008; *Mouchet*, 2011]. The UVic ESCM consists of an ocean general circulation model (Modular Ocean Model, Version 2) with a resolution of 3.6° longitude and 1.8° latitude and coupled to a vertically integrated two-dimensional energy-moisture balance model of the atmosphere including a parameterization of geostrophic wind stress anomalies, a dynamic-thermodynamic sea ice model, a land surface scheme, a dynamic global vegetation model [*Meissner et al.*, 2003b], a marine carbon cycle model [*Schmittner et al.*, 2008], and a sediment model [*Meissner et al.*, 2012].

[6] First, some idealized experiments are performed with LOVECLIM and the UVic ESCM under constant Last Glacial Maximum (LGM, 21 ka B.P.) boundary conditions. A presentation of the performances of LOVECLIM and the UVic ESCM under LGM conditions can be found in previous publications [*Menviel et al.*, 2008a; *Meissner et al.*, 2003a]. As the sea level was lower during glacial times, the Bering Strait is closed in all the experiments. Our study focuses on the marine carbon cycle response to a shutdown of the AMOC. To avoid the marine carbon cycle responding to changes in terrestrial carbon, the terrestrial carbon reservoir is kept constant at its LGM value in all the experiments performed here. We run two experiments in which the AMOC is shut down through the addition

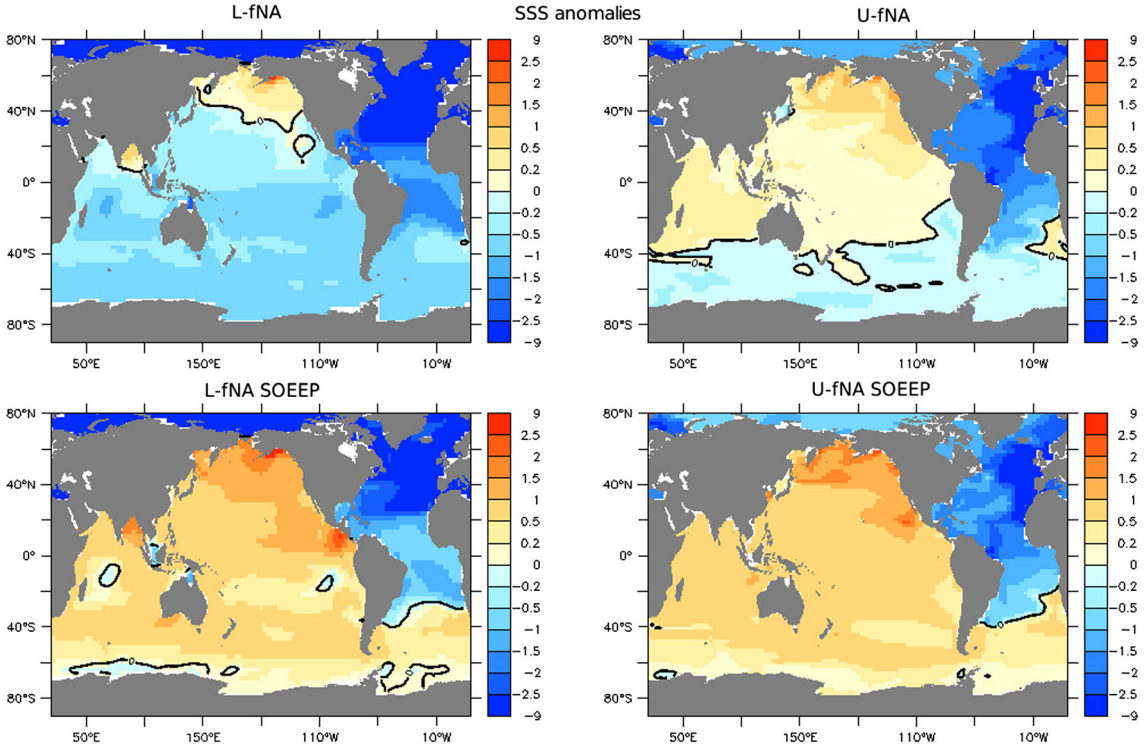

Figure 3. Sea Surface Salinity anomalies: SSS (g/kg) anomalies with respect to the LGM control run averaged for model years 1990–2000 for (top) standard meltwater experiments and (bottom) meltwater experiments with a negative freshwater input in the Southern Ocean and the EEP for (left) LOVECLIM and (right) the UVic ESCM.

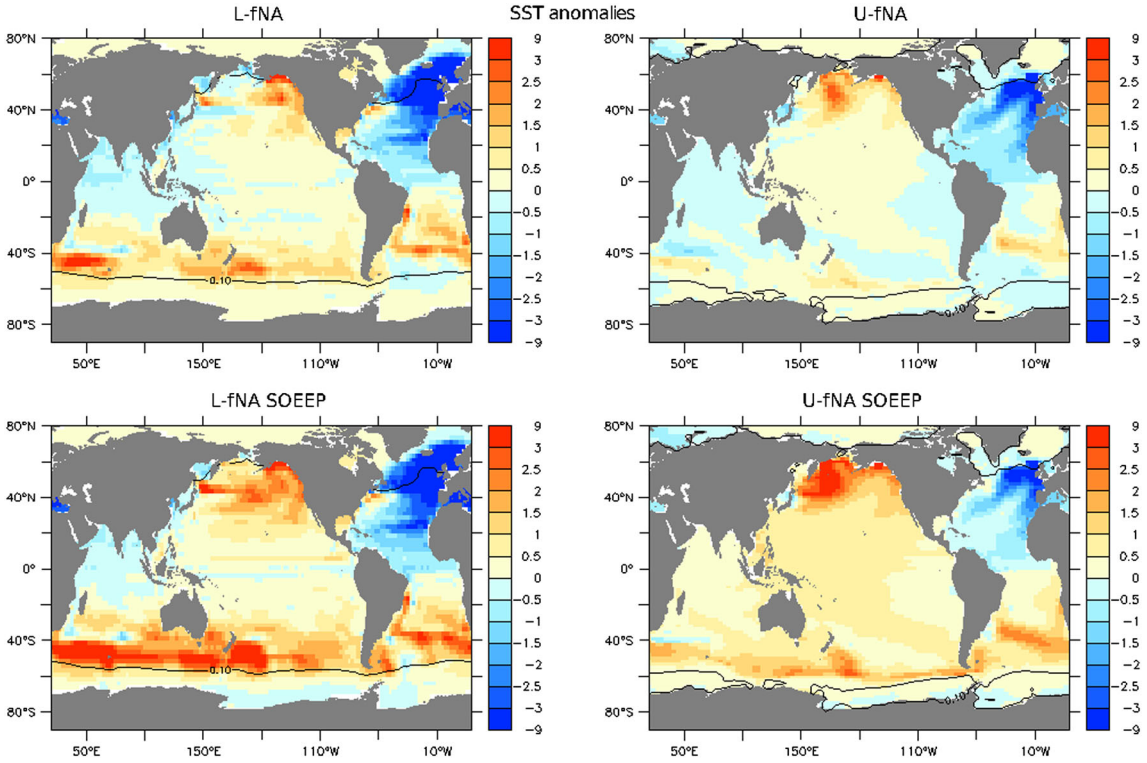

Figure 4. Sea surface temperature anomalies: Same as Figure 3 but for SST (°C) anomalies. Overlaid is the 0.1 m sea ice thickness contour for austral winter (JJA).

of 0.1 Sverdrup (Sv) (1 Sv = 10^6 m^3/s) freshwater in the North Atlantic (55°W–10°W, 50°N–65°N) for 2000 years (L-fNA and U-fNA, respectively, performed with LOVECLIM and the UVic ESCM). Due to a combination of experimental design, model resolution, and other model biases, we hypothesize that standard meltwater experiments might generate anomalously low surface salinity in the Pacific Ocean. Therefore, two experiments are forced with an additional compensating salt flux (0.15 Sv for LOVECLIM and 0.1 Sv for the UVic ESCM) over the Southern Ocean (40°S–50°S, 0°E–120°E; 50°S–62°S, 120°E–280°E) and the Eastern Equatorial Pacific (0°N–11°N, 104°W–88°W) ($L\text{-}fNA_{SOEEP}$ and $U\text{-}fNA_{SOEEP}$) during the first 2000 years. To simulate the recovery of the AMOC, a salt flux (0.2 Sv) is added in the North Atlantic between model years 2000 and 3000.

[7] To test the robustness of our results a set of sensitivity experiments is also performed with both LOVECLIM and the UVic ESCM adding 0.2 Sv of freshwater in the North Atlantic for 1000 years. In some experiments, a salt flux (0–0.2 Sv) is also added over the Southern Ocean, the Eastern Equatorial Pacific, and/or the North Pacific (Table S1). In addition, further experiments are performed with LOVECLIM under different initial conditions and employing a range of values for the Gent and McWilliams thickness diffusion coefficient (GM: 0 m^2/s, 200 m^2/s (default value), 700 m^2/s, and 1400 m^2/s) (Table S3).

[8] In a second step, a transient experiment covering Heinrich stadial 4 (HS4, ~40 ka B.P.) is performed with LOVECLIM. The model is first integrated with boundary conditions for the period 42 ka B.P.: forcing includes orbital parameters [*Berger*, 1978], ice sheet topography and albedo [*Abe-Ouchi et al.*, 2007], a closed Bering Strait, and an atmospheric CO_2 content of 210 ppmv. Two transient experiments (L-HS4 and $L\text{-}HS4_{SOEEP}$) are then integrated from 42 ka B.P. to 38.5 ka B.P. with all the transient forcing described above and with prognostic atmospheric CO_2. In the setup used here, even though the vegetation is interactive, the land carbon is set constant at its 42 ka B.P. value. Both experiments are forced with freshwater fluxes into the North Atlantic designed to fit the sea surface temperature (SST) record from the Iberian margin (Figure 9a, black line) [*Martrat et al.*, 2007; *Menviel et al.*, 2013]. In experiment $L\text{-}HS4_{SOEEP}$, a negative freshwater flux (–0.15 Sv) is also applied in the Eastern Equatorial Pacific and the Southern Ocean between 39.6 and 39.3 ka B.P. (Figure 9a, dashed blue line).

2.2. Sea Surface Salinity Estimates

[9] In Figure 1h we estimate sea surface salinity (SSS) anomalies in the South Pacific Ocean core MD03-2611 [*Calvo et al.*, 2007] by subtracting from planktic $\delta^{18}O_{plk}$ changes in global ice volume ($\delta^{18}O_{ice}$) [*Waelbroeck et al.*, 2002; *Lisiecki et al.*, 2008]: $\delta^{18}O_c=\delta^{18}O_{plk}-\delta^{18}O_{ice}$; taking out the SST contribution [*Shackleton*, 1974] estimated by alkenone content $U^{K'}_{37}$: $\delta^{18}O_w=(SST-16.9+4*\delta^{18}O_c)/4$; and finally using the $\delta^{18}O_w$-salinity relationship based on surface ocean data [*Schmidt et al.*, 1999] for latitudes 30°S–40°S: $\Delta SSS=1.5678*\delta^{18}O_w+34.53$. In Figure 9, we use a similar method to estimate SSS in core MD97-2120 [*Pahnke et al.*, 2003], but using the $\delta^{18}O_w$-salinity relationship for latitudes 40°S–50°S: $\Delta SSS=1.465*\delta^{18}O_w+34.00$.

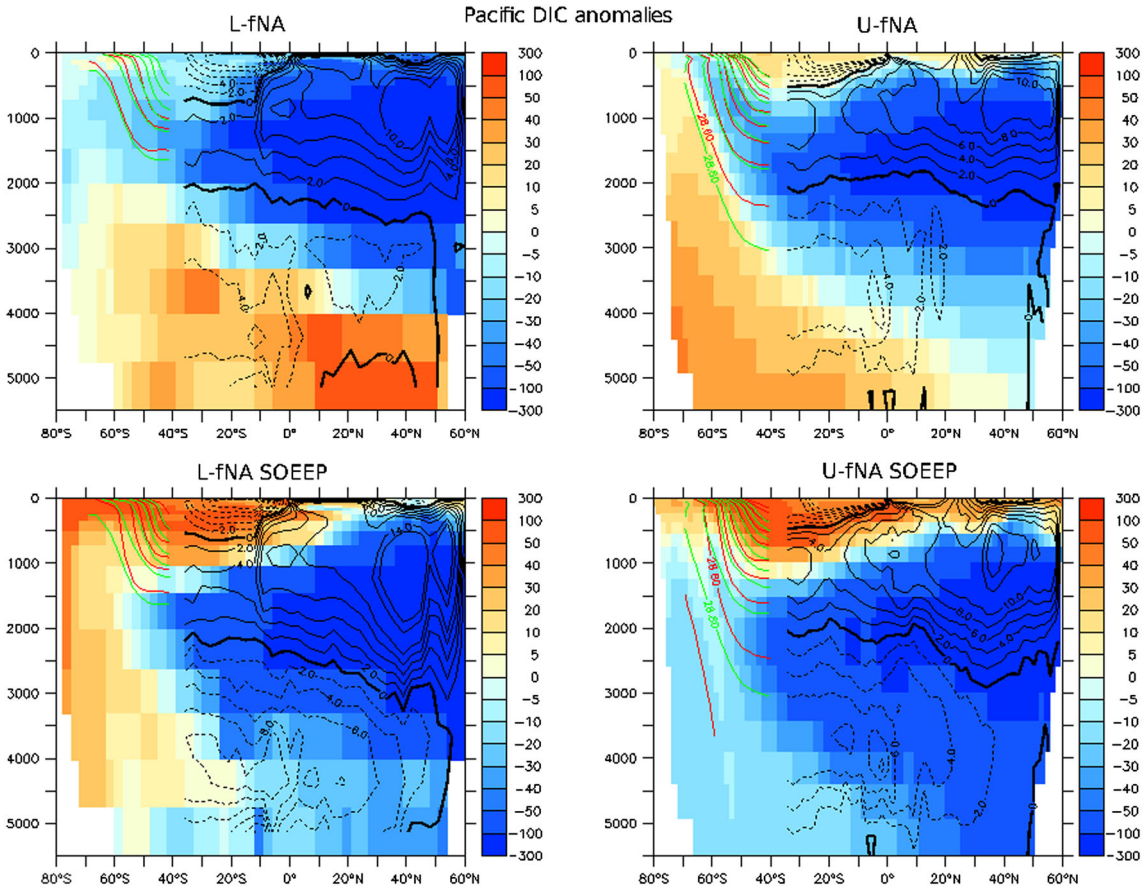

Figure 5. DIC anomalies averaged over the Pacific basin and meridional overturning stream function: Latitude-depth DIC anomalies (μmol/L) compared to the LGM control run, averaged over the Pacific basin for model years 1990–2000 for (top) standard meltwater experiments performed with (left) LOVECLIM and (right) the UVic ESCM, as well as (bottom) meltwater experiments with enhanced AABW transport. Overlaid are the meridional overturning stream function (Sv, black) integrated over the Indo-Pacific basin and the Ross Sea, as well as the South Pacific annual mean isopycnal surfaces (green) compared to the LGM control run (blue).

2.3. pCO_2 Decomposition

[10] The factors controlling surface water pCO_2 and, ultimately, atmospheric CO_2, include changes in SSS, SST, dissolved inorganic carbon (DIC), and alkalinity (ALK) [*Sarmiento and Gruber*, 2006; *D'Orgeville et al.*, 2011]. We use the following equations to decompose the pCO_2 signal in Figure 2:

$$\Delta pCO_2 = \Delta pCO_{2DIC} + \Delta pCO_{2ALK} + \Delta pCO_{2SST} + \Delta pCO_{2SSS} \quad (1)$$

[11] For DIC, ALK, and SSS:

$$\Delta pCO_{2X} = \Delta X^* \gamma_X^* pCO_{2Ref}/\overline{X} \quad (2)$$

where $\overline{X}$ represents the mean DIC, ALK, or SSS value and γ_{DIC}, γ_{ALK}, and γ_{SSS} are equal to 10, –9.4, and 1, respectively [*Sarmiento and Gruber*, 2006].

[12] The temperature contribution is derived from

$$\Delta pCO_{2SST} = \exp(\Delta SST^* \gamma_{SST})^* pCO_{2Ref} - pCO_{2Ref} \quad (3)$$

where γ_{SST} is equal to 0.0423.

3. Results

3.1. Idealized LGM Experiments

[13] The cessation of NADW formation under constant LGM conditions in LOVECLIM and the UVic ESCM leads to an oceanic carbon reservoir increase and to a 4 ppmv atmospheric CO_2 decrease (Table 1 and Figure 1l). Figure 2 (d, blue and black lines) shows that the pCO_2 decrease due to the AMOC shutdown may be partially attributed to the enhanced CO_2 solubility in seawater due to the global freshening of the surface waters (Figure 2c, blue and black lines). The addition of freshwater into the North Atlantic to simulate a shutdown of the AMOC leads to strong negative SSS anomalies across the entire Atlantic basin as well as throughout the Southern Ocean (Figure 3). A shutdown of the AMOC also leads to a classic SST seesaw response in both LOVECLIM and the UVic ESCM, with a strong cooling in the North Atlantic and warming in the Southern Ocean (Figure 4). The warming simulated over the Southern Ocean is, however, much greater in LOVECLIM than in the UVic ESCM.

[14] An increase in surface DIC leads to a greater oceanic partial pressure of CO_2; however, an increase in surface

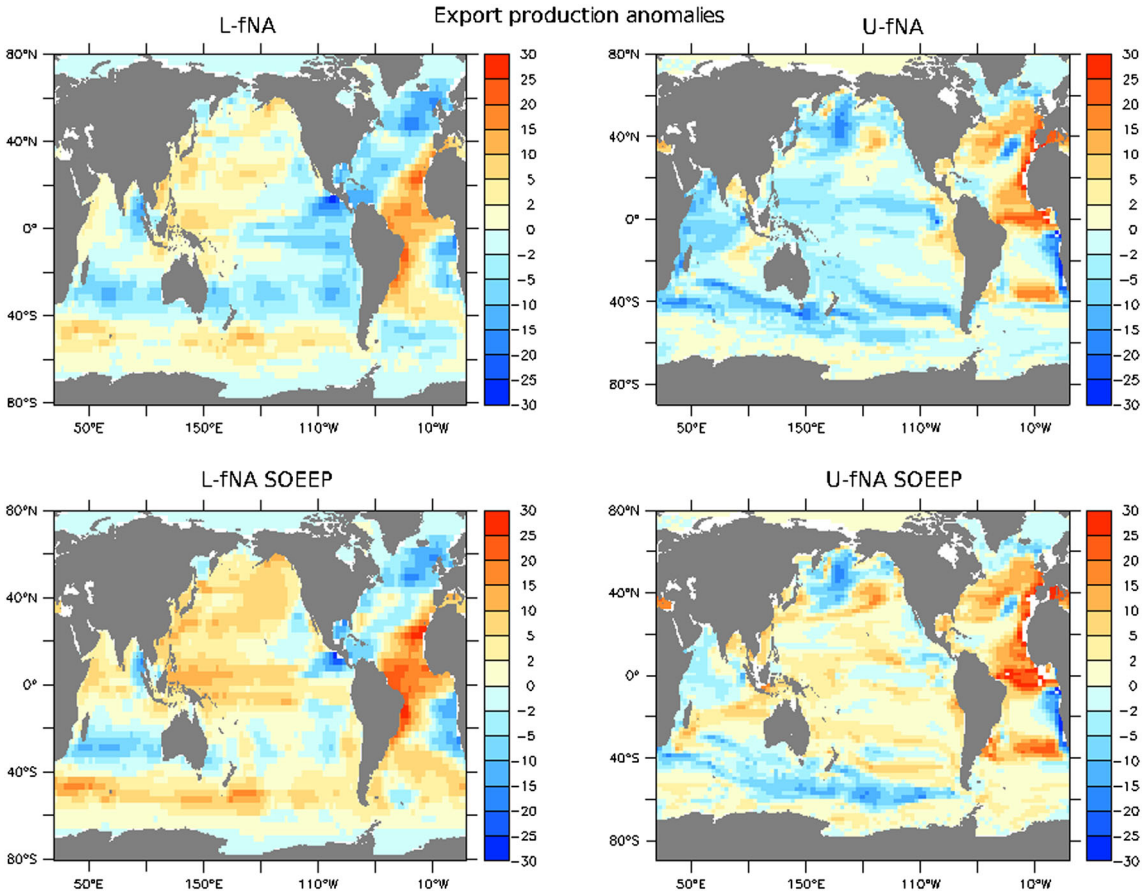

Figure 6. Export production anomalies: Same as Figure 3 but for export production anomalies ($gC/m^2/yr$).

alkalinity decreases oceanic pCO_2. The imbalance between changes in surface DIC and ALK explains a large part of the atmospheric pCO_2 decrease in the first 1000 years of the experiments (Figures 2e and 2f). For example, in LOVECLIM, the initial pCO_2 decrease ($\leq$500 years) is partly due to a low DIC anomaly in the surface waters, resulting from the greater stratification in the North Atlantic.

[15] Due to the weaker overturning in the Atlantic Ocean, the residence time of deep waters increases, thus leading to a greater DIC content in the deep Atlantic Ocean ($\sim$200 GtC after 2000 yrs, Table 1). On the other hand, through oceanic and atmospheric teleconnections a weak AMOC leads to the formation of NPDW [*Saenko et al.*, 2004; *Okazaki et al.*, 2010]. The greater ventilation of the North Pacific Ocean (Figure 1C) leads to a loss of DIC in the North Pacific intermediate and deep waters (Table 1 and Figure 5).

[16] In agreement with previous studies [*Schmittner*, 2005; *Obata*, 2007; *Chikamoto et al.*, 2012; *Mariotti et al.*, 2012], reduced global and $CaCO_3$ export production (up to –9%) are simulated in both models (Figures 1E, grey lines and 6), mainly due to greater stratification over the Atlantic region and to a weaker upwelling in the eastern Pacific region (not shown). However, stratification further leads to a 6% and 12% increase in nutrient utilization efficiency ($1-\overline{PO_{4\,surface}}/\overline{PO_{4\,deep}}$) in LOVECLIM and the UVic ESCM, respectively, thus enhancing the efficiency of the biological pump and effectively trapping carbon in the ocean interior.

[17] Even though quantitative SSS reconstructions are associated with large uncertainties [*Legrande and Schmidt*, 2011], equatorial and South Pacific SSS most likely increased during Heinrich stadials 1 and 4 [*Stott et al.*, 2002; *Pahnke et al.*, 2003; *Calvo et al.*, 2007; *Leduc et al.*, 2007], in contradiction with our initial results (Figures 1h, 1H, and 3). It has been suggested that as the AMOC weakened, moisture transport from the Atlantic to the Pacific across Central America was reduced [*Richter and Xie*, 2010] and that the East Asian Summer Monsoon weakened [*Wang et al.*, 2001]. These processes, best represented in multilevel high-resolution atmospheric General Circulation Models, would contribute to increased surface salinity in the Pacific Ocean, with significant consequences for Pacific deep and bottom water formation. It is hypothesized that due to the coarse resolution and simplified atmospheric physics of the models used in this study, the SSS in the Pacific Ocean might be underestimated.

[18] We perform further Heinrich-type experiments in which we try to rectify for the low surface salinity anomalies in the Pacific Ocean. In experiments L-fNA_{SOEEP} and U-fNA_{SOEEP}, the surface salinity in the Southern Pacific Ocean now increases by about 0.5 g/kg, consistent with paleoproxy records for Heinrich stadials [*Pahnke et al.*, 2003; *Calvo et al.*, 2007] (Figures 1h and 1H, green lines). Atmospheric CO_2 increases by respectively 10 and 25 ppmv in LOVECLIM and the UVic ESCM due to lower CO_2

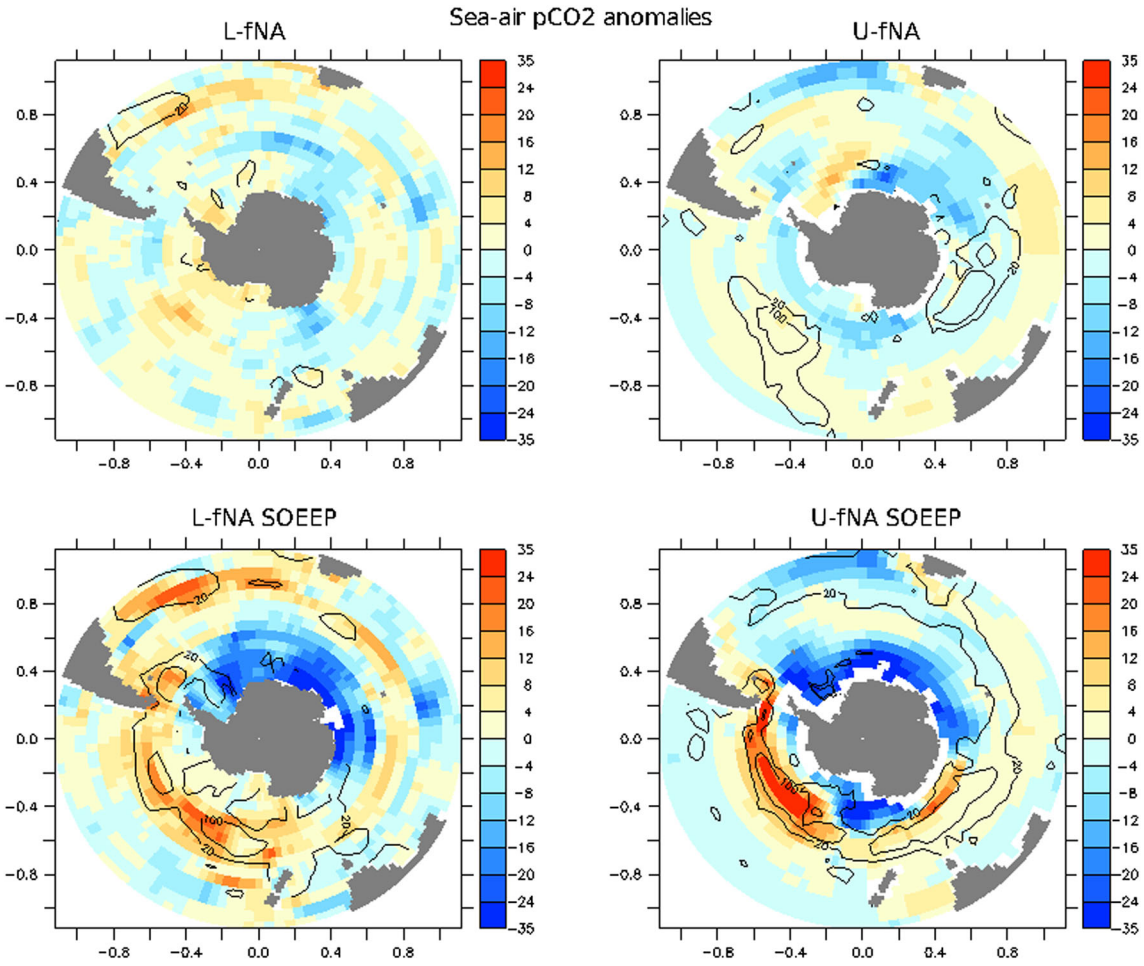

Figure 7. Sea-air ΔpCO_2 and mixed layer depth anomalies: Sea-air ΔpCO_2 anomalies (μatm) for (top) standard meltwater experiments and (bottom) for experiments in which the AABW and NPDW transport strengthen, performed with (left) LOVECLIM and (right) the UVic ESCM. Contours indicate austral winter mixed layer depth anomalies (m). Data shown correspond to the largest rate of pCO_2 change: i.e., model years 190–200 and 390–400 for LOVECLIM, and 490–500 and 390–400 for the UVic ESCM. Red colors represent CO_2 outgassing into the atmosphere.

solubility as well as enhanced ventilation of the deep and bottom waters of the Pacific Ocean (Figures 1 and 2).

[19] During the AMOC shutdown, the surface waters get slightly saltier (0–0.2 g/kg) and warmer (0–0.4°C), thus lowering CO_2 solubility (Figures 2c and 2d, green and red lines). In addition, the SSS increase leads to a strengthening of AABW in the Pacific Ocean by 3 to 5 Sv (Figure 1D, blue lines). AABW is calculated here as the maximum strength of the overturning in the abyssal cell at 35°S. Stronger NPDW induces a warming at the surface of the North Pacific Ocean, particularly in its eastern part (Figure 4). As described elsewhere [*Saenko et al.*, 2004; *Okazaki et al.*, 2010; *Menviel et al.*, 2012b], formation of NPDW weakens the Indonesian throughflow transport while strengthening the Kuroshio Current, thus enhancing the transport of warm tropical waters to the Northwest Pacific. A strengthening of AABW further enhances the warming at middle- and high-latitudes in the Southern Hemisphere (Figure 4) via enhanced poleward heat transport. In LOVECLIM, enhanced AABW strengthens the ACC by ~15% (not shown). The Antarctic Circumpolar Current (ACC) is not only zonal but has a meridional component at certain longitudes and thus plays a role in transporting heat poleward [*Volkov et al.*, 2010]. In addition, the East Australian Current and the Brazil Current strengthen by ~15% (not shown), thus bringing more warm and salty water to the South Pacific and South Atlantic.

[20] The combination of strong AABW and NPDW leads to enhanced ventilation of the Pacific basin (Figure 5). While the deep Atlantic basin is still a sink of carbon (Table 1), the transport of DIC-rich deep Pacific waters (Table 1 and Figure 5) to the surface and CO_2 outgassing into the atmosphere is thus significantly enhanced (Figure 7). The more saline surface waters (Figure 3) induce deep convection primarily in the Pacific sector of the Southern Ocean as indicated by the strong (up to 300 m) deepening of the austral winter mixed layer depth (Figure 7) and a steepening of the isopycnals south of 50°S (Figure 5). In the Pacific sector of the Southern Ocean, DIC is advected equatorward by Ekman transport and CO_2 outgassing thus occurs south of 58°S. In LOVECLIM, the DIC-rich waters are also transported by the ACC to the South Atlantic and the South Indian Oceans, where the CO_2 flux to the

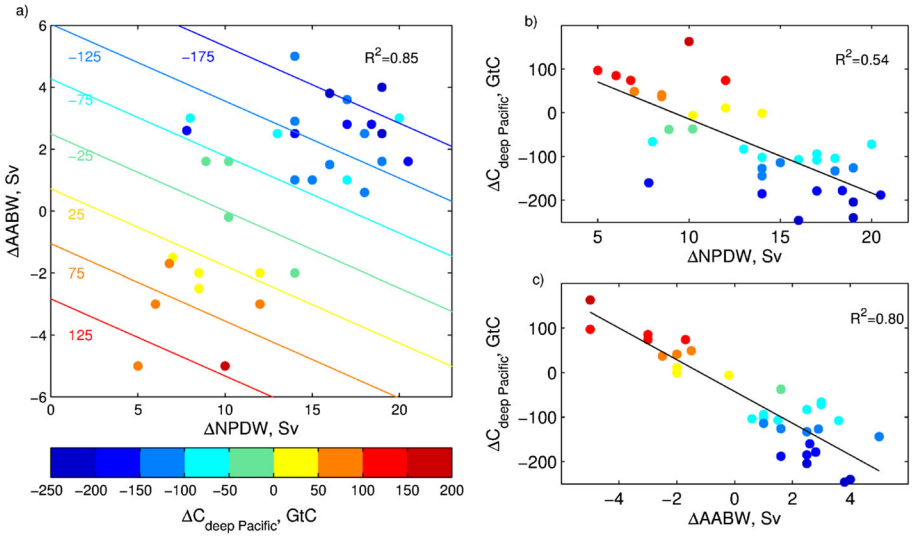

Figure 8. Relation between deep Pacific carbon, Antarctic Bottom Water, and North Pacific Deep Water: (a) Deep Pacific carbon content anomalies (GtC, ≥2000m for LOVECLIM and ≥2200m for the UVic ESCM) as a function of the change in Antarctic Bottom Water (AABW, Sv) and North Pacific Deep Water (NPDW, Sv). The stronger AABW and NPDW are, the more carbon is ventilated out of the Pacific Ocean. (b) Deep Pacific carbon content anomalies (GtC) as a function of the change in NPDW (Sv). (c) Deep Pacific carbon content anomalies (GtC) as a function of the change in AABW (Sv). Each point represents the result of a sensitivity experiment for model years 990–1000 (Tables S2 and S3). The multiple linear regression analysis of deep Pacific carbon content anomalies versus change in AABW and NPDW leads to a correlation coefficient, R^2, of 0.85. Most of the variability is due to changes in AABW (R^2=0.80). In Figure 8a, the colored contour lines indicate values obtained if the linear relationship held perfectly.

atmosphere is enhanced at 40°S–50°S. In the UVic ESCM, the ACC transport is weaker than in LOVECLIM and the Southern Ocean SST (Figure 4) does not increase as much; therefore, all the CO_2 outgassing occurs in the Pacific Ocean.

[21] In LOVECLIM, greater ventilation of the Southern Ocean enhances opal production over the South Atlantic Ocean, in good agreement with a record from the South Atlantic (Figures 1f and 1F, magenta lines) [*Anderson et al.*, 2009]. The global export production also now increases by 10–15% in both models (Figure 1E, red lines).

[22] It should be noted that in the UVic ESCM, once the AMOC is shut down it does not recover without the addition of a negative buoyancy flux over the North Atlantic Ocean (e.g., freshwater extraction from the ocean). Instead, NPDW formation strengthens and after the freshwater forcing in the North Atlantic has stopped, the surface salinity of the Pacific Ocean increases, thus leading to a strengthening of AABW formation. For example, in experiments performed with the UVic ESCM and forced with a 0.2 Sv freshwater input in the North Atlantic for 500 years (see supporting information), the AABW transport first weakens by 1.8 Sv then slowly increases up to 2 Sv compared to the initial state. As a result atmospheric CO_2 first decreases by 5 ppmv and then increases in phase with AABW to reach a pCO_2 anomaly of +5 ppmv. This result is similar to the one obtained by *Schmittner et al.* [2007]; however, it is lower than the 22 ppmv atmospheric CO_2 increase simulated by *Schmittner and Galbraith* [2008] under the same forcing conditions. *Schmittner and Galbraith* [2008] show that the atmospheric CO_2 rise simulated in their experiments was due to the global increase in the preformed phosphate (PO_{4Pref}) inventory [*Ito and Follows*, 2005]. Here we argue that these variations in PO_{4Pref} are mainly due to changes in the ventilation of the Pacific bottom and deep water masses, i.e., enhanced AABW and to a lesser extent enhanced NPDW transport. In LOVECLIM, changes in atmospheric CO_2 content also reflect changes in AABW and NPDW transport; however, there is no clear link with changes in PO_{4Pref} inventory. This is partly due to the small PO_{4Pref} gradient in the deep Atlantic basin under LGM conditions. In addition, as already shown in *Menviel et al.* [2008b], the biological pump in the Southern Ocean is very reactive in LOVECLIM. The enhanced Southern Ocean ventilation leads to a 30% increase in export production over the Southern Ocean in LOVECLIM, whereas Southern Ocean export production decreases by 7% in the UVic ESCM (Figure 6).

[23] Figures 2e and 2f show the different contributions of DIC and ALK to the pCO_2 change. The individual contributions of DIC and ALK are larger in LOVECLIM than in the UVic ESCM, due to the greater gradient of both DIC and ALK between the surface and the deep (not shown). The resulting pCO_2 anomalies, however, depend on the relative contribution of DIC over alkalinity. The imbalance between alkalinity and DIC is much larger for the UVic ESCM thus contributing to about 18 ppmv pCO_2 increase. This is mainly due to the much greater DIC gradient between the surface and the deep compared to the vertical alkalinity gradient (not shown). DIC and alkalinity gradients are set by the biological and carbonate pumps in the ocean thus indicating stronger biological and carbonate pumps in LOVECLIM than in the UVic ESCM.

3.2. Changes in AABW and NPDW and Their Impact on Deep Pacific Carbon

[24] Our results highlight the importance of changes in AABW and NPDW and their impact on oceanic and atmospheric carbon. Depending on the bottom and deep water mass transports in the Pacific Ocean, the ocean can act either as a sink or as a source of carbon through an Atlantic-Pacific seesaw. The stronger the transport of NPDW and AABW in the Pacific Ocean, the more carbon is released from the deep Pacific through the Southern Ocean to the atmosphere. Figure 8 shows the relationship between changes in deep Pacific carbon, AABW and NPDW transport obtained from a series of sensitivity experiments (LOVECLIM and the UVic ESCM, including different freshwater forcing and Gent McWilliams parametrization coefficients, Tables S1 and S3.)

[25] Deep Pacific carbon release primarily depends on AABW transport, as indicated by a 0.80 correlation coefficient between these two model integral metrics. A multilinear regression analysis including both AABW and NPDW slightly improves the correlation (R^2=0.85), thus corroborating the role of stronger NPDW in outgassing CO_2. However, this regression underestimates the role of NPDW as it only takes into account changes in carbon below 2000 m depth. Stronger NPDW ventilates North Pacific intermediate waters and is thus a main factor in controlling the Pacific carbon budget (Figure 5). This is also confirmed by the results of meltwater experiments performed with the coupled Atmospheric Ocean General Circulation model MIROC 3.2 [*Chikamoto et al.*, 2012], in which atmospheric CO_2 decreases by 15 ppmv. The atmospheric CO_2 decrease is partly due to the enhanced CO_2 solubility due to colder and fresher surface waters. In addition, the NPDW transport is negligible so that carbon can be stored in both the Atlantic and Pacific Oceans.

3.3. Validation of the Mechanism for Heinrich Stadial 4

[26] We now run a fully coupled transient simulation of HS4 from 40.5 to 38.5 ka B.P. forcing LOVECLIM with a freshwater input in the North Atlantic (Figure 9, black lines). A shutdown of the AMOC during HS4 leads to simulated air temperature and SST anomalies over Greenland and the Iberian margin in reasonable agreement with paleoproxy records [*Huber et al.*, 2006; *Bard*, 2002; *Martrat et al.*, 2007; *Elliot et al.*, 2002; *Cacho et al.*, 1999]. However, the simulated SSS over the Eastern Equatorial Pacific (EEP) and the Southern Ocean decrease by 0.4 g/kg and there is no significant atmospheric CO_2 increase simulated between 39.75 and 39.4 ka B.P.

[27] We run an additional fully coupled transient simulation of HS4, which includes a freshwater flux in the North Atlantic and a salt flux over the Southern Ocean, and the EEP to compensate for the low salinity anomaly over the Pacific Ocean, equivalent to the experiments described in section 3.1. In this new experiment, the forcing is equivalent to a 12 m sea level rise, compared to the 20 m sea level rise in the first experiment. The forcing applied in both experiments is consistent with sea level rise estimates of 10–25 m for HS4 [*Chappell*, 2002; *Siddall et al.*, 2003]. The agreement between modeling results and paleoproxies is still good over Greenland and the North Atlantic (Figure 9, blue lines). Notably, in the new experiment, the SSS in the EEP and the

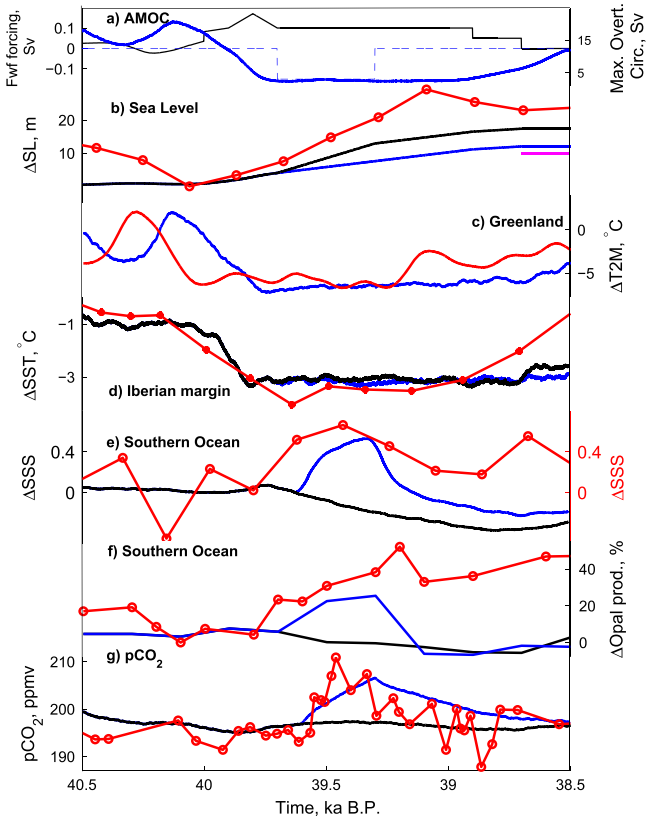

Figure 9. Model-paleoproxy comparison for Heinrich stadial 4: Results of transient experiments L-HS4 (black) and L-HS4$_{SOEEP}$ (blue) compared to paleoproxy records (red). Time series of (a) Maximum overturning circulation in the North Atlantic (Sv) (blue) as well as freshwater forcing (Sv) in the North Atlantic for both experiments (black) and over the Southern Ocean and the EEP for L-HS4$_{SOEEP}$ (dashed blue); (b) Changes in sea level (m) resulting from the forcing applied compared to the estimates from the Red Sea (red) [*Siddall et al.*, 2003] and from Papua New Guinea (magenta) [*Chappell*, 2002]; (c) Greenland air temperature (°C) as simulated and as recorded in the North Greenland Ice Core Project (NGRIP) ice core [*Huber et al.*, 2006]; (d) SST anomalies (°C) as simulated and as recorded in marine sediment core MD95-2042 off the Iberian margin [*Martrat et al.*, 2007]; (e) SSS anomaly in the South Pacific Ocean (175°E–260°E, 35°S–48°S) compared to the SSS anomaly estimated from $\delta^{18}O$ and SST from marine sediment core MD97-2120 [*Pahnke et al.*, 2003]; (f) opal production anomaly (%) averaged over the South Atlantic Ocean (50°W–20°E, 42°S–60°S) compared to the opal flux anomaly (%) record from the South Atlantic marine sediment core TNO57-14PC [*Anderson et al.*, 2009]; (g) atmospheric CO_2 (ppmv) as simulated and as recorded in Byrd ice core, Antarctica [*Ahn and Brook*, 2008].

Southern Ocean increases by 2.0 and 0.6 g/kg, respectively, in better agreement with paleoproxy records [*Leduc et al.*, 2007; *Pahnke et al.*, 2003]. In addition, the opal production in the Southern Ocean increases significantly (+25%), consistent with a proxy record from the South Atlantic [*Anderson et al.*, 2009]. Saltier surface conditions over the Southern and North Pacific Oceans lead to enhanced

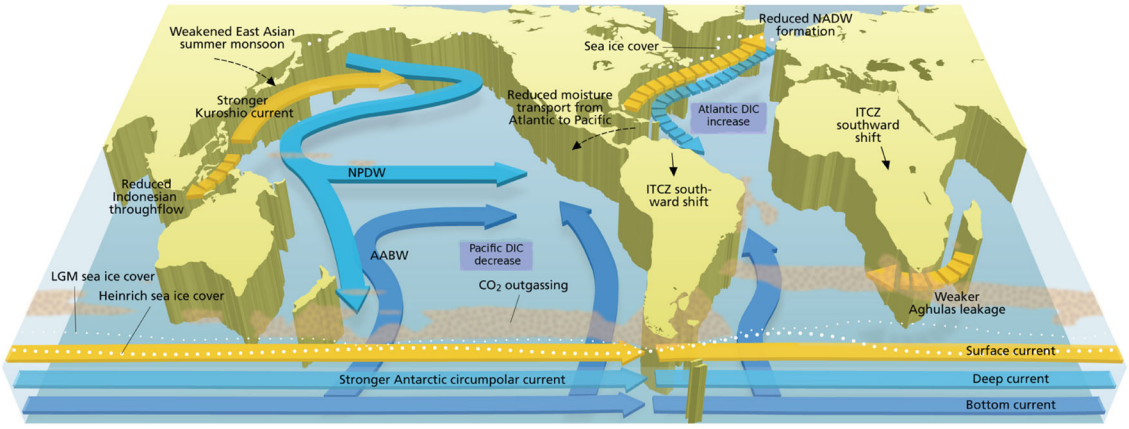

Figure 10. Mechanism for CO_2 release during Heinrich stadials 4 and 1: A shutdown of the AMOC leads to a greater heat transport to the south and a sea ice retreat in the Southern Ocean. The North Atlantic cooling induces a southward shift of the Intertropical Convergence Zone, a weakening of the East Asian Summer Monsoon and a reduced moisture transport from the Atlantic to the Pacific over Central America. Due to an increased salinity at the surface of the Pacific Ocean, the transport of AABW and NPDW is enhanced, thus effectively releasing deep Pacific carbon into the atmosphere through the Southern Ocean. The deep carbon reservoir is reduced in the Pacific, while it increases in the Atlantic Ocean.

formation and transport of NPDW and AABW in the Pacific Ocean, thus effectively ventilating deep Pacific carbon through the Southern Ocean. We simulate a 10 ppmv atmospheric CO_2 increase over 300 years, close to the 15 ppmv atmospheric CO_2 rise observed in the Byrd ice core [*Ahn and Brook*, 2008; *Ahn et al.*, 2012]. Our results suggest that enhanced deep and bottom water mass transport in the Pacific Ocean could have played a critical role in raising atmospheric CO_2 during HS4.

4. Discussion and Conclusions

[28] Our results show that solubility effects as well as changes in the deep and bottom water mass transport in the Pacific Ocean are the primary control of the marine carbon cycle during a shutdown of the Atlantic Meridional Overturning Circulation (AMOC). Depending on the strength of Antarctic Bottom Water (AABW) and North Pacific Deep Water (NPDW), the ocean can act either as a sink or as a source of carbon through an Atlantic-Pacific seesaw. The stronger the transport of NPDW and AABW in the Pacific Ocean, the more carbon is released from the deep and intermediate Pacific to the atmosphere. In addition, changes in NPDW and AABW have an influence on the climate of the Pacific region [*Menviel et al.*, 2010, 2012b] and are thus also important for changes in terrestrial carbon.

[29] Our fully coupled transient simulation of HS4 has further shown that an increase in AABW and NPDW transport during the AMOC shutdown could have played a major role in shaping the observed atmospheric CO_2 increase (Figure 9) [*Ahn and Brook*, 2008]. Around 40 ka B.P., the Antarctic ice sheet was close to its maximum extent and presumably covered most of present-day AABW formation regions: the Weddell and Ross Seas [*Denton and Hughes*, 2002; *Pollard and DeConto*, 2009]. At the onset of HS4, meltwater in the North Atlantic slows down NADW formation. Reduced moisture transport from the Atlantic to the Pacific across Central America increases the salinity in the Eastern Equatorial Pacific [*Leduc et al.*, 2007; *Richter and Xie*, 2010; *Peterson et al.*, 2000] (Figure 10). A weaker East Asian Summer monsoon [*Tada et al.*, 1999; *Wang et al.*, 2001] also increases the salinity in the North Pacific. Finally, it has been suggested that a stronger Kuroshio Current coupled to a reduced Indonesian throughflow could lead to the formation of NPDW [*Okazaki et al.*, 2010]. Through the Stommel feedback [*Stommel*, 1961], the NPDW strengthening leads to an increase in the salinity of North Pacific waters. In the Southern Ocean, the increased heat flux due to the AMOC weakening and the strong Southern Hemispheric high-latitude insolation results in a sea ice retreat. In addition, positive salinity anomalies that arise in the Eastern Equatorial Pacific can be advected to the South Pacific and across the ACC by eddies. We hypothesize that the sea ice retreat associated with greater surface salinity induces deep convection around 60°S primarily in the Pacific sector of the Southern Ocean [*Meissner et al.*, 2008], thus releasing carbon stored in the deep Pacific Ocean. Both deep convection and rising atmospheric CO_2 provide a positive feedback, further enhancing the sea ice retreat. A reduction in the density gradient between the North and South Pacific could also enhance the AABW transport in the Pacific Ocean [*Watson and Naveira Garabato*, 2006]. Such a mechanism (Figure 10) operating during HS4 is consistent with paleoproxy records as it induces a carbonate ion rise in the deep Indian and Pacific Oceans [*Yu et al.*, 2010, 2013], increases surface salinity in the Pacific Ocean [*Leduc et al.*, 2007; *Pahnke et al.*, 2003], enhances AABW transport [*Piotrowski et al.*, 2005], and leads to greater upwelling of nutrient-rich waters in the Southern Ocean (Figure 9) [*Anderson et al.*, 2009], thus effectively increasing atmospheric CO_2 [*Ahn and Brook*, 2008].

[30] A similar mechanism occurring during HS1 is also consistent with paleoproxy records as it lowers atmospheric $\delta^{13}CO_2$ [*Schmitt et al.*, 2012; *Tschumi et al.*, 2011], decreases the ventilation age of deep Southern Ocean waters [*Skinner et al.*, 2010], and enhances mixing of Upper and Lower Circumpolar Deep Waters [*Burke and Robinson*, 2012]. It is also consistent with a decrease in atmospheric

$\Delta^{14}C$ [*Huiskamp and Meissner*, 2012; *Matsumoto and Yokoyama*, 2013]. Antarctic ice cores record an atmospheric CO_2 increase of 33 ppmv at the beginning of the last deglaciation and across HS1 [*Monnin et al.*, 2001]. Our results suggest that enhanced AABW and NPDW transport during HS1 could have accounted for about 30% of the observed atmospheric CO_2 increase. Such an atmospheric pCO_2 increase during HS1 would contribute to the last deglaciation atmospheric pCO_2 increase alongside other mechanisms [*Menviel et al.*, 2012a].

[31] Our study suggests that an AMOC shutdown associated with a strengthening of the Pacific AABW and NPDW during HS4 and possibly HS1 led to a release of carbon into the atmosphere in agreement with paleoproxy records. Depending on the background conditions and the magnitude of the event, not all Heinrich stadials might be associated with enhanced AABW transport. This could explain the lack of noticeable atmospheric CO_2 increase during HS2, for example.

[32] **Acknowledgments.** This project was supported by the Australian Research Council. Model experiments were performed on a computational cluster owned by the Faculty of Science of the University of New South Wales as well as on a cluster from the NCI National Facility at the Australian National University. K.J. Meissner acknowledges funding from the ARC Future Fellowship program (FT100100443) and M. England funding from the ARC Laureate Fellowship program (FL100100214). We thank Editor H. Päelike and A. Schmittner, as well as an anonymous reviewer for their constructive comments.

References

Abe-Ouchi, A., T. Segawa, and F. Saito (2007), Climatic conditions for modelling the Northern Hemisphere ice sheets throughout the Ice Age cycle, *Clim. Past*, *3*, 423–438.

Ahn, J., and E. J. Brook (2008), Atmospheric CO_2 and climate on millennial time scales during the last glacial period, *Science*, *322*, 83–85, doi:10.1126/science.1160832.

Ahn, J., E. J. Brook, A. Schmittner, and K. J. Kreutz (2012), Abrupt change in atmospheric CO_2 during the last ice age, *Geophys. Res. Lett.*, *39*, L18711, doi:10.1029/2012GL053018.

Anderson, R. F., S. Ali, L. I. Bradtmiller, S. H. H. Nielsen, M. Q. Fleisher, B. E. Anderson, and L. H. Burckle (2009), Wind-driven upwelling in the Southern Ocean and the deglacial rise in Atmospheric CO_2, *Science*, *323*, 1443–1448.

Bard, E. (2002), Abrupt climate changes over millennial time scales: Climate shock, *Phys. Today*, *55*, 32–38.

Bereiter, B., D. Lüthi, M. Siegrist, S. Schüpbach, T. F. Stocker, and H. Fischer (2012), Mode of change of millennial CO2 variability during the last glacial cycle associated with a bipolar marine carbon seesaw, *Proc. Natl. Acad. Sci.*, *109*, 9755–9760, doi:10.1073/pnas.1204069109.

Berger, A. (1978), Long term variations of daily insolation and Quaternary climate change, *J. Atmos. Sci.*, *35*, 2362–2367.

Blunier, T., and E. J. Brook (2001), Timing of millennial-scale climate change in Antarctica and Greenland during the last glacial period, *Science*, *291*, 109–112.

Bond, G. (1993), Correlations between climate records from North Atlantic sediments and Greenland ice, *Nature*, *365*, 143–147.

Bouttes, N., D. M. Roche, and D. Paillard (2012), Systematic study of the impact of fresh water fluxes on the glacial carbon cycle, *Clim. Past*, *8*, 589–607.

Bozbiyik, A., M. Steinacher, F. Joos, T. F. Stocker, and L. Menviel (2011), Fingerprints of changes in the terrestrial carbon cycle in response to large reorganizations in ocean circulation, *Clim. Past*, *7*, 319–338.

Burke, A., and L. F. Robinson (2012), The Southern Ocean's role in carbon exchange during the last deglaciation, *Science*, *335*, 557–561.

Cacho, I., J. O. Grimalt, C. Pelejero, M. Canals, F. J. Sierro, J. A. Flores, and N. Shackleton (1999), Dansgaard-Oeschger and Heinrich event imprints in Alboran Sea paleotemperatures, *Paleoceanography*, *14*, 698–705.

Calvo, E., C. Pelejero, P. De Deckker, and G. A. Logan (2007), Antarctic deglacial pattern in a 30 kyr record of sea surface temperature offshore South Australia, *Geophys. Res. Lett.*, *34*, L13707, doi:10.1029/2007GL029937.

Chappell, J. (2002), Sea level changes forced ice breakouts in the last glacial cycle: New results from coral terraces, *Quat. Sci. Rev.*, *21*, 1229–1240.

Chikamoto, M. O., L. Menviel, A. Abe-Ouchi, R. Ohgaito, A. Timmermann, Y. Okazaki, N. Harada, A. Oka, and A. Mouchet (2012), Variability in North Pacific intermediate and deep water ventilation during Heinrich events in two coupled climate models, *Deep Sea Res. Part II*, *61–64*, 114–126.

Condron, A., and P. Winsor (2011), A subtropical fate awaited freshwater discharged from glacial Lake Agassiz, *Geophys. Res. Lett.*, *38*, L03705, doi:10.1029/2010GL046011.

Dansgaard, W., S. J. Johnsen, and H. B. Clausen (1993), Evidence for general instability of past climate from a 250-kyr ice-core record, *Nature*, *364*, 218–220.

Denton, G. H., and T. J. Hughes (2002), Reconstructing the Antarctic Ice Sheet at the Last Glacial Maximum, *Quat. Sci. Rev.*, *21*, 193–202.

Deplazes, G., et al. (2013), Links between tropical rainfall and North Atlantic climate during the last glacial period, *Nat. Geosci.*, *6*, 213–217, doi:10.1038/NGEO1712.

D'Orgeville, M., M. H. England, and W. P. Sijp (2011), Buffered versus non-buffered ocean carbon reservoir variations: Application to the sensitivity of atmospheric CO_2 to ocean circulation changes, *Geophys. Res. Lett.*, *38*, L24603, doi:10.1029/2011GL049823.

Elliot, M., L. Labeyrie, G. Bond, E. Cortijo, J.-L. Turon, N. Tisnerat, and J.-C. Duplessy (1998), Millennial-scale iceberg discharges in the Irminger Basin during the last glacial period: Relationship with the Heinrich events and the environmental settings, *Paleoceanography*, *13*, 433–446.

Elliot, M., L. Labeyrie, and J.-C. Duplessy (2002), Changes in North Atlantic deep-water formation associated with the Dansgaard-Oeschger temperature oscillations (60-10 ka), *Quat. Sci. Rev.*, *21*, 1153–1165.

Gherardi, J. M., L. Labeyrie, J. F. McManus, R. Francois, L. C. Skinner, and E. Cortijo (2005), Evidence from the Northeastern Atlantic basin for variability in the rate of the meridional overturning circulation through the last deglaciation, *Earth Planet. Sci. Lett.*, *240*, 710–723.

Goosse, H., et al. (2010), Description of the Earth system model of intermediate complexity LOVECLIM version 1.2, *Geosci. Model Dev.*, *3*, 603–633.

Grousset, F. E., C. Pujol, L. Labeyrie, G. Auffret, and A. Boelaert (2000), Were the North Atlantic Heinrich events triggered by the behavior of the European ice sheets?, *Geology*, *28*, 123–126.

Heinrich, H. (1988), Origin and consequences of cyclic ice rafting in the northeast Atlantic Ocean during the past 130,000 years, *Quat. Res.*, *29*, 142–152.

Hemming, S. R. (2004), Heinrich events: Massive late Pleistocene detritus layers of the North Atlantic and their global climate imprint, *Rev. Geophys.*, *42*, RG1005, doi:10.1029/2003RG000128.

Huber, C., M. Leuenberger, R. Spahni, J. Flückiger, J. Schwander, T. F. Stocker, S. Johnsen, A. Landais, and J. Jouzel (2006), Isotope calibrated Greenland temperature record over Marine Isotope Stage 3 and its relation to CH4, *Earth Planet. Sci. Lett.*, *243*, 504–519.

Huiskamp, W. N., and K. J. Meissner (2012), Oceanic carbon and water masses during the Mystery Interval: A model-data comparison study, *Paleoceanography*, *27*, PA4206, doi:10.1029/2012PA002368.

Ito, T., and M. J. Follows (2005), Preformed phosphate, soft tissue pump and atmospheric CO_2, *J. Mar. Res.*, *63*, 813–839.

Köhler, P., F. Joos, S. Gerber, and R. Knutti (2005), Simulated changes in vegetation distribution, land carbon storage, and atmospheric CO_2 in response to a collapse of the North Atlantic thermohaline circulation, *Clim. Dyn.*, *25*, 689–708.

Leduc, G., L. Vidal, K. Tachikawa, F. Rostek, C. Sonzogni, L. Beaufort, and E. Bard (2007), Moisture transport across Central America as a positive feedback on abrupt climatic changes, *Nature*, *445*, 908–911.

Legrande, A., and G. A. Schmidt (2011), Water isotopologues as a quantitative paleosalinity proxy, *Paleoceanography*, *26*, PA3225, doi:10.1029/2010PA002043.

Lisiecki, L. E., M. E. Raymo, and W. B. Curry (2008), Atlantic overturning responses to Late Pleistocene climate forcings, *Nature*, *456*, 85–88.

Marchal, O., T. F. Stocker, F. Joos, A. Indermühle, T. Blunier, and J. Tschumi (1999), Modelling the concentration of atmospheric CO^2 during the Younger Dryas climate event, *Clim. Dyn*, *15*, 341–354.

Mariotti, V., L. Bopp, A. Tagliabue, M. Kageyama, and D. Swingedouw (2012), Marine productivity response to Heinrich events: A model-data comparison, *Clim. Past*, *8*, 1581–1598.

Martrat, B., J. O. Grimalt, N. J. Shackleton, L. de Abreu, M. A. Hutterli, and T. F. Stocker (2007), Four climate cycles of recurring deep and surface water destabilizations on the Iberian margin, *Science*, *317*, 502–507.

Matsumoto, K., and Y. Yokoyama (2013), Atmospheric $\Delta^{14}C$ reduction in simulations of Atlantic overturning circulation shutdown, *Global Biogeochem. Cycles*, *27*, 296–304, doi:10.1002/gbc.20035.

McManus, J. F., R. Francois, J. M. Gherardi, L. D. Keigwin, and S. Brown-Leger (2004), Collapse and rapid resumption of Atlantic meridional circulation linked to deglacial climate changes, *Nature*, *428*, 834–837.

Meissner, K. J., A. Schmittner, A. J. Weaver, and J. F. Adkins (2003a), The ventilation of the North Atlantic Ocean during the Last Glacial Maximum: A comparison between simulated and observed radiocarbon ages, *Paleoceanography*, *18*(2), 1023, doi:10.1029/2002PA000762.

Meissner, K. J., A. J. Weaver, H. D. Matthews, and P. M. Cox (2003b), The role of land surface dynamics in glacial inception: A study with the UVic Earth System Model, *Clim. Dyn.*, *21*, 515–537.

Meissner, K. J., M. Eby, A. J. Weaver, and O. A. Saenko (2008), CO_2 threshold for millennial-scale oscillations in the climate system: Implications for global warming scenarios, *Clim. Dyn.*, *30*, 161–174.

Meissner, K. J., B. I. McNeil, M. Eby, and E. C. Wiebe (2012), The importance of the terrestrial weathering feedback for multimillennial coral reef habitat recovery, *Global Biogeochem. Cycles*, *26*, GB3017, doi:10.1029/2011GB004098.

Menviel, L. (2008), Climate-carbon cycle interactions on millennial to glacial timescales as simulated by a model of intermediate complexity, LOVECLIM, PhD thesis, University of Hawai'i, http://myweb.science.unsw.edu.au/lauriemenviel/Menvielthesis2008.pdf.

Menviel, L., A. Timmermann, A. Mouchet, and O. Timm (2008a), Meridional reorganizations of marine and terrestrial productivity during Heinrich events, *Paleoceanography*, *23*, PA1203, doi:10.1029/2007PA001445.

Menviel, L., A. Timmermann, A. Mouchet, and O. Timm (2008b), Climate and marine carbon cycle response to changes in the strength of the southern hemispheric westerlies, *Paleoceanography*, *23*, PA4201, doi:10.1029/2007PA001604.

Menviel, L., A. Timmermann, A. Mouchet, and O. Timm (2010), Climate and biogeochemical response to a rapid melting of the West-Antarctic Ice Sheet during interglacials and implications for future climate, *Paleoceanography*, *25*, PA4231, doi:10.1029/2009PA001892.

Menviel, L., F. Joos, and S. P. Ritz (2012a), Modeling atmospheric CO_2, stable carbon isotope and marine carbon cycle changes during the last glacial-interglacial cycle, *Quat. Sci. Rev*, *56*, 46–68.

Menviel, L., A. Timmermann, A. Mouchet, O. Timm, A. Abe-Ouchi, M. O. Chikamoto, N. Harada, R. Ohgaito, and Y. Okazaki (2012b), Removing the North Pacific halocline: Effects on global climate, ocean circulation and the carbon cycle, *Deep Sea Res. Part II*, *61-64*, 106–113.

Menviel, L., A. Timmermann, T. Friedrich, and M. H. England (2013), Hindcasting the continuum of Dansgaard-Oeschger variability: Mechanisms, patterns and timing, *Clim. Past Discuss.*, *9*, 4771–4806.

Monnin, E., A. Indermühle, A. Dällenbach, J. Flückiger, B. Stauffer, T. F. Stocker, D. Raynaud, and J.-M. Barnola (2001), Atmospheric CO_2 concentration over the last glacial termination, *Science*, *291*, 112–114.

Mouchet, A. (2011), A 3D model of ocean biogeochemical cycles and climate sensitivity studies, PhD thesis, Université de Liège, Lìege, Belgium, http://hdl.handle.net/2268/98995.

Obata, A. (2007), Climate-carbon cycle model response to freshwater discharge into the North Atlantic, *J. Clim.*, *20*, 5962–5976.

Okazaki, Y., A. Timmermann, L. Menviel, N. Harada, A. Abe-Ouchi, M. Chikamoto, A. Mouchet, and H. Asahi (2010), Deep water formation in the North Pacific during the Last Glacial termination, *Science*, *329*, 200–204.

Pahnke, K., R. Zahn, H. Elderfield, and M. Schulz (2003), 340,000-year centennial-scale marine record of Southern Hemisphere climatic oscillation, *301*, 948–952.

Parrenin, F., V. Masson-Delmotte, P. Köhler, D. Raynaud, D. Paillard, J. Schwander, C. Barbante, A. Landais, A. Wegner, and J. Jouzel (2013), Synchronous change of atmospheric CO_2 and Antarctic temperature during the last deglacial warming, *Science*, *339*, 1060–1063.

Peterson, L. C., G. H. Haug, K. A. Hughen, and U. Rohl (2000), Rapid changes in the hydrologic cycle of the Tropical Atlantic during the Last Glacial, *Science*, *290*, 1947–1951.

Piotrowski, A. M., S. L. Goldstein, S. R. Hemming, and R. G. Fairbanks (2005), Temporal relationships of carbon cycling and ocean circulation glacial boundaries, *Science*, *307*, 1933–1938.

Pollard, D., and R. M. DeConto (2009), Modelling West Antarctic ice sheet growth and collapse through the past five million years, *Nature*, *458*, 329–332.

Richter, I., and S.-P. Xie (2010), Moisture transport from the Atlantic to the Pacific basin and its response to North Atlantic cooling and global warming, *Clim. Dyn.*, *35*, 551–566.

Saenko, O. A., A. Schmittner, and A. J. Weaver (2004), The Atlantic-Pacific seesaw, *J. Climate*, *17*, 2033–2038.

Sarmiento, J. L., and N. Gruber (2006), *Ocean Biogeochemical Dynamics*, pp. 526, Princeton Univ. Press, Princeton, N. J.

Schmidt, G. A., G. R. Bigg, and E. J. Rohling (1999), Global Seawater Oxygen-18 Database, v1.21. http://data.giss.nasa.gov/o18data/.

Schmitt, J., et al. (2012), Carbon isotope constraints on the deglacial CO_2 rise from ice cores, *Science*, *136*, 711–714.

Schmittner, A. (2005), Decline of the marine ecosystem caused by a reduction in the Atlantic overturning circulation, *Nature*, *434*, 628–633.

Schmittner, A., and E. D. Galbraith (2008), Glacial greenhouse-gas fluctuations controlled by ocean circulation changes, *Nature*, *456*, 373–376.

Schmittner, A., E. J. Brook, and J. Ahn (2007), Impact of the ocean's overturning circulation on atmospheric CO2, in *Ocean Circulation: Mechanisms and Impacts, Geophys. Monogr. Ser.,* vol. 173, edited by A. Schmittner, J. C. H. Chiang, and S. R. Hemming, pp. 315–334, AGU, Washington, D. C.

Schmittner, A., A. Oschlies, H. D. Matthews, and E. D. Galbraith (2008), Future changes in climate, ocean circulation, ecosystems, and biogeochemical cycling simulated for a business-as-usual CO_2 emission scenario until year 4000 AD, *Global Biogeochem. Cycles*, *22*, GB1013, doi:10.1029/2007GB002953.

Scholze, M., W. Knorr, and M. Heimann (2003), Modelling terrestrial vegetation dynamics and carbon cycling for an abrupt climatic change event, *Holocene*, *13*, 327–333.

Shackleton, N. J. (1974), *Les methodes quantitatives d'etude des variations du climat au cours du Pleistocene,* vol. 219, Editions du Centre national de la recherche scientifique (CNRS), Paris.

Siddall, M., E. J. Rohling, A. Almogi-Labin, C. Hemleben, D. Meischner, I. Schmelzer, and D. A. Smeed (2003), Sea-level fluctuations during the last glacial cycle, *Nature*, *423*, 853–858.

Skinner, L. C., S. Fallon, C. Waelbroeck, E. Michel, and S. Barker (2010), Ventilation of the deep Southern Ocean and deglacial CO_2 rise, *Science*, *328*, 1147–1151.

Snoeckx, H., F. Grousset, M. Revel, and A. Boelaert (1999), European contribution of ice-rafted sand to Heinrich layers H3 and H4, *Mar. Geol.*, *158*, 197–208.

Spence, P., O. A. Saenko, W. Sijp, and M. H. England (2013), North Atlantic climate response to Lake Agassiz drainage at coarse and ocean eddy-permitting resolutions, *J. Climate*, *26*, 2651–2667, doi:10.1175/JCLI–D–11–00683.1.

Stommel, H. M. (1961), Thermohaline convection with two stable regimes of flow, *Tellus*, *13*, 224–230.

Stott, L. C., C. Poulsen, S. Lund, and R. Thunell (2002), Super ENSO and global climate oscillations at millenial time scales, *Science*, *279*, 222–226.

Tada, R., T. Irino, and I. Koizumi (1999), Land-ocean linkages over orbital and millennial time-scales recorded in late Quaternary sediments of the Japan Sea, *Paleoceanography*, *14*, 236–247.

Tschumi, T., F. Joos, M. Gehlen, and C. Heinze (2011), Deep ocean ventilation, carbon isotopes, marine sedimentation and the deglacial CO_2 rise, *Clim. Past*, *7*, 771–800.

Vidal, L., L. Labeyrie, E. Cortijo, M. Arnold, J. C. Duplessy, E. Michel, S. Becque, and T. C. E. van Weering (1997), Evidence for changes in the North Atlantic Deep Water linked to meltwater surges during the Heinrich events, *Earth Planet. Sci. Lett.*, *146*, 13–27.

Volkov, D. L., L.-L. Fu, and T. Lee (2010), Mechanisms of the meridional heat transport in the Southern Ocean, *Ocean Dyn.*, *60*, 791–801.

Waelbroeck, C., L. Labeyrie, J.-C. Duplessy, J. F. McManus, K. Lambeck, E. Balbon, and M. Labracherie (2002), Sea-level and deep water temperature changes derived from benthic foraminifera isotopic records, *Quat. Sci. Rev.*, *21*, 295–305.

Wang, Y. J., H. Cheng, R. L. Edwards, Z. S. An, J. Y. Wu, C. C. Shen, and J. A. Dorale (2001), A high-resolution absolute-dated Late Pleistocene monsoon record from Hulu Cave, China, *Science*, *294*, 2345–2348.

Watson, A. J., and A. C. Naveira Garabato (2006), The role of Southern Ocean mixing and upwelling in glacial-interglacial atmospheric CO_2 change, *Tellus B*, *58*, 73–87.

Weaver, A. J., et al. (2001), The UVic Earth System Climate Model: Model description, climatology, and applications to past, present and future climates, *Atmos. Ocean*, *4*, 361–428.

Yu, J., W. S. Broecker, H. Elderfield, Z. Jin, J. McManus, and F. Zhang (2010), Loss of carbon from the deep sea since the Last Glacial Maximum, *Science*, *330*, 1084–1087.

Yu, J., R. F. Anderson, Z. Jin, J. W. B. Rae, B. N. Opdyke, and S. M. Eggins (2013), Responses of the deep ocean carbonate system to carbon reorganization during the Last Glacial-interglacial cycle, *Quat. Sci. Rev.*, *76*, 39–52.